ACS APPLIED MATERIALS & INTERFACES

Research Article

www.acsami.org

Impact of Soft Annealing on the Performance of Solution-Processed Amorphous Zinc Tin Oxide Thin-Film Transistors

Pradipta K. Nayak,[†] Mohamed N. Hedhili,[‡] Dongkyu Cha,[‡] and H. N. Alshareef*[,†]

[†]Materials Science and Engineering and [‡]Imaging and Characterization Laboratory, King Abdullah University of Science and Technology (KAUST), Thuwal, 23955-6900, Saudi Arabia

ABSTRACT: It is demonstrated that soft annealing duration strongly affects the performance of solution-processed amorphous zinc tin oxide thin-film transistors. Prolonged soft annealing times are found to induce two important changes in the device: (i) a decrease in zinc tin oxide film thickness, and (ii) an increase in oxygen vacancy concentration. The devices prepared without soft annealing exhibited inferior transistor performances, in comparison to devices in which the active channel layer (zinc tin oxide) was subjected to soft annealing. The highest saturation field-effect mobility—5.6 $cm^2\ V^{-1}\ s^{-1}$ with a drain-to-source on−off current ratio (I_{on}/I_{off}) of 2×10^8—was achieved in the case of devices with 10-min soft-annealed zinc tin oxide thin films as the channel layer. The findings of this work identify soft annealing as a critical parameter for the processing of chemically derived thin-film transistors, and it correlates device performance to the changes in material structure induced by soft annealing.

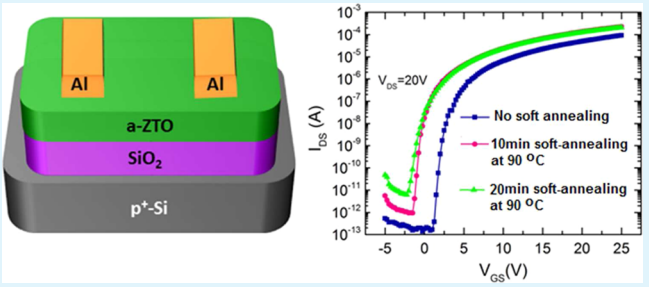

KEYWORDS: *thin film transistor, field-effect, amorphous oxide semiconductor, zinc tin oxide, soft annealing, solution-process*

INTRODUCTION

Transparent semiconducting oxide thin film transistors (TFTs) have attracted much attention recently, as manifested by a huge increase in the number of active research groups and materials being investigated.[1] The primary interest in oxide TFTs is due to their potential use in flat-panel displays (FPDs) and other electronic device applications, where they can replace amorphous silicon TFTs, which are known for their low mobility (<1 $cm^2\ V^{-1}\ s^{-1}$).[2−6] One area that has seen promising progress is the solution processing of metal oxide thin films for TFT applications. In particular, high-performance TFTs using zinc oxide (ZnO),[7,8] indium oxide,[9] indium zinc oxide (IZO),[10,11] zinc tin oxide (ZTO),[12,13] indium zinc tin oxide (IZTO),[14] and indium gallium zinc oxide (IGZO)[15−17] thin films as the channel layers have been reported using the simple sol−gel spin coating technique. The growing interest in solution deposition techniques is mainly due to their various advantages, such as simplicity, homogeneity and excellent compositional control at the molecular level, low cost, and high throughput, which enables the fabrication of high-performance and low-cost electronic devices. In the case of spin coating as a deposition method, a low-temperature soft annealing of wet films is often required just after the spin coating process to drive out the solvent. Without such annealing process, defects and/or bubbles are formed in the oxide film, which degrades film uniformity and device performances. It has been reported that soft annealing helps to improve the bonding and adhesion between the film and the substrate below it.[18] Moreover, it has also been reported that the conductivity of the oxide thin films can be improved by preannealing of wet films before the final high-temperature annealing.[19] However, prolonged duration of soft annealing may lead to a significant increase in background carrier density; hence, it will be difficult to fabricate a TFT with controlled characteristics.[20] Furthermore, it has also been reported that elemental diffusion from the channel layer into the gate dielectric depends on the quality of the dielectric.[21] Thus, it is very important to optimize the duration of the soft annealing process before the high-temperature annealing step, in order to obtain films with fewer defects and better device performances.

In the present work, the effect of soft annealing duration on the physical and chemical properties of the channel layer and resultant device performance of amorphous, chemically derived ZTO thin film transistors is investigated.

EXPERIMENTAL SECTION

The precursor solution for the deposition of amorphous ZTO semiconducting channel layers was prepared by dissolving tin(II) chloride and zinc acetate dihydrate in 2-methoxyethanol. The molar ratio of zinc (0.1 M) to tin (0.1 M) was fixed as 1:1 and equimolar of (0.2 M) ethanolamine was added to the mixed solution as the stabilizing agent. The mixed solution was stirred at 50 °C in air for 1 h and aged for ∼24 h. Heavily doped *p*-type silicon substrates with 100 nm thermally developed silicon dioxide (SiO_2) were used as the bottom gate and dielectric, respectively. The silicon/SiO_2 substrates were cleaned ultrasonically by acetone, isopropanol and deionized water and then dried by nitrogen gas flow. The cleaned substrates were

Received: December 25, 2012
Accepted: April 1, 2013
Published: April 1, 2013

   dx.doi.org/10.1021/am303235z | *ACS Appl. Mater. Interfaces* 2013, 5, 3587−3590

exposed to oxygen plasma (30 W) for 3 min using a Harrick plasma (PDC-002) cleaner to enhance the hydrophilicity of the SiO_2 surface. One layer of the ZTO precursor solution was spun on SiO_2 surfaces at a rotation speed of 4000 rpm for 30 s in air. After spin coating, the wet precursor films were placed on a preheated hot plate at 90 °C in air for different durations (0, 10, and 20 min) and then subjected to rapid annealing at 500 °C for 1 h in an air atmosphere, using a tube furnace idling at the desired process temperature. The TFTs containing the ZTO channel layers soft annealed on the hot plate for 0, 10, and 20 min will hereafter be called as ZTO-0, ZTO-10, and ZTO-20, respectively. Aluminum (70 nm) source and drain electrodes with channel width (W) and length (L) of 500 and 100 μm, respectively, were deposited using electron beam evaporation and shadow mask. Crystallinity and cross-sectional images of ZTO films was investigated using a transmission electron microscopy (TEM) system (Titan ST, FEI). X-ray reflectivity (XRR) patterns of the ZTO films were obtained by a Bruker D8 Discover X-ray diffractometer using Cu Kα radiation. The chemical composition of the ZTO films was analyzed by X-ray photoelectron spectroscopy (XPS) using an Axis Ultra DLD spectrometer (Kratos Analytical, U.K.). The current−voltage characteristics of the ZTO TFTs were performed using a semiconductor characterization system (Keithley, Model 4200-SCS) and a microprobe station (Cascade Microtech, Model Summit-11600 AP).

RESULTS AND DISCUSSION

Figure 1a shows a schematic of the TFT device structure used in this study. Figures 1b and 1c show the output and transfer characteristics, respectively, of the TFTs with ZTO channel layers processed using different soft annealing times. It can be seen from Figure 1b that the output characteristics of all the TFTs exhibit clear pinch-off and excellent saturation behavior with an enhanced mode of operation. The drain to source on-current was found to increase after a soft annealing of 10 min, but slightly decreased in the case of 20-min soft annealing of the TFT, which can also be clearly seen from the transfer characteristics curves in Figure 1c. The field-effect mobility (μ_{sat}) of the TFTs was estimated in the saturation regime operation of the transfer curve (Figure 1c), using the following equation:

$$I_{DS,sat} = \left(\frac{W}{2L}\right)\mu_{sat}C_{ox}(V_{GS} - V_{TH})^2 \quad (1)$$

where I_{DS} is the drain-to-source current; V_{GS} is the gate-to-source voltage; V_{TH} is the threshold voltage; W and L are the channel width and length, respectively; and C_{ox} is the capacitance per unit area of the gate dielectric. The values of μ_{sat}, the drain-to-source current on−off ratio (I_{on}/I_{off}), and V_{TH} for the TFT with ZTO-0 as the channel layer were found to be 2.8 $cm^2\ V^{-1}\ s^{-1}$, 5×10^8, and 5.4 V, respectively. The value of μ_{sat} increased in the case of the TFTs made using soft-annealed ZTO channel layers. Specifically, the μ_{sat} values for the ZTO-10 and ZTO-20 TFTs were found to be 5.6 and 4.8 $cm^2\ V^{-1}\ s^{-1}$, respectively. The threshold voltage of the ZTO-10 and ZTO-20 TFTs were measured to be 3.3 and 2.9 V, respectively. A gradual increase in the drain-to-source off-current was observed as the soft annealing time was increased, as seen in the transfer characteristic curve (Figure 1c). The I_{on}/I_{off} ratio in case of the ZTO-20 was ∼1 order of magnitude less than the ZTO-0 and ZTO-10 TFTs. The values of subthreshold swing ($s = \partial V_{DS}/\partial \log_{10} I_{DS}$) for the ZTO-0, ZTO-10, and ZTO-20 TFTs were found to be 0.28, 0.27, and 0.50 V dec^{-1}, respectively.

The increase in subthreshold swing (s) and the drain-to-source off-current (I_{off}) in the case of the TFT with ZTO-20 as the channel layer indicates that the channel conductivity of the ZTO-20 TFT is higher than that of the ZTO-0 and ZTO-10 TFTs. We calculated the channel resistance of the different ZTO TFTs from the I_{DS} vs V_{DS} plot measured at zero gate-to-source voltage. The channel resistances of the ZTO-0, ZTO-10, and ZTO-20 TFTs were found to be 1.5×10^{10}, 3.7×10^8, and 1.5×10^8 Ω, respectively. Thus, the increase in I_{off} and s correlate well with the increased channel conductivity, due to the increase in soft annealing time.

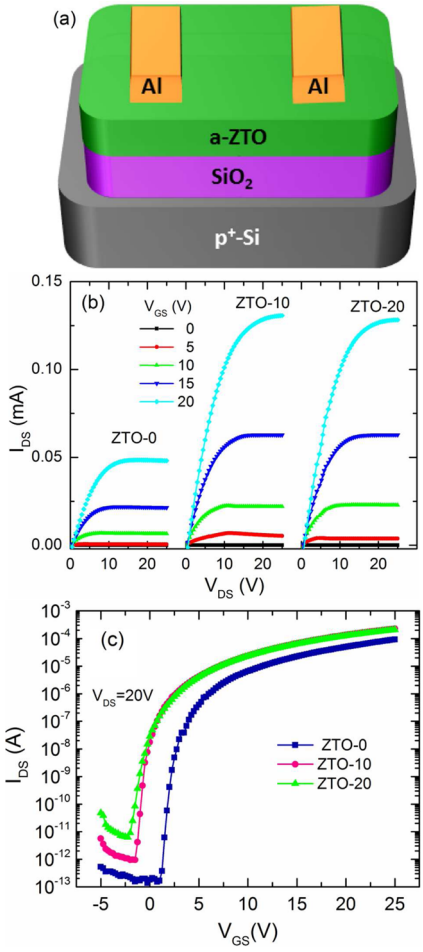

Figure 1. (a) Schematic of the device structure, as well as graphics showing the (b) output and (c) transfer characteristic curves of the TFTs with ZTO channel layers soft-annealed for 0 min (ZTO-0), 10 min (ZTO-10), and 20 min (ZTO-20).

The material properties of ZTO thin films deposited on Si/SiO_2 were investigated using different analytical techniques to understand the mechanism by which soft annealing times modify the performance of ZTO TFTs. Figures 2a−c show the cross-sectional TEM images of ZTO films prepared using different soft annealing times. Although all the ZTO films were prepared under the same deposition conditions, a decrease in film thickness was observed as the soft annealing duration increased. From the TEM cross-sectional images, the thickness of the ZTO-0, ZTO-10, and ZTO-20 films were found to be 13.1, 8.9, and 6.2 nm, respectively. No regular atomic arrangement was found from the cross-sectional TEM images, suggesting the formation of amorphous ZTO films. Furthermore, the amorphous nature of the ZTO films was also confirmed from the Fourier transform patterns of the corresponding ZTO films (results are not shown here). The XRR patterns of the different ZTO films deposited on p^+-Si/SiO_2 surfaces are shown in Figure 2d. The Kiessig fringes which

dx.doi.org/10.1021/am303235z | ACS Appl. Mater. Interfaces 2013, 5, 3587−3590

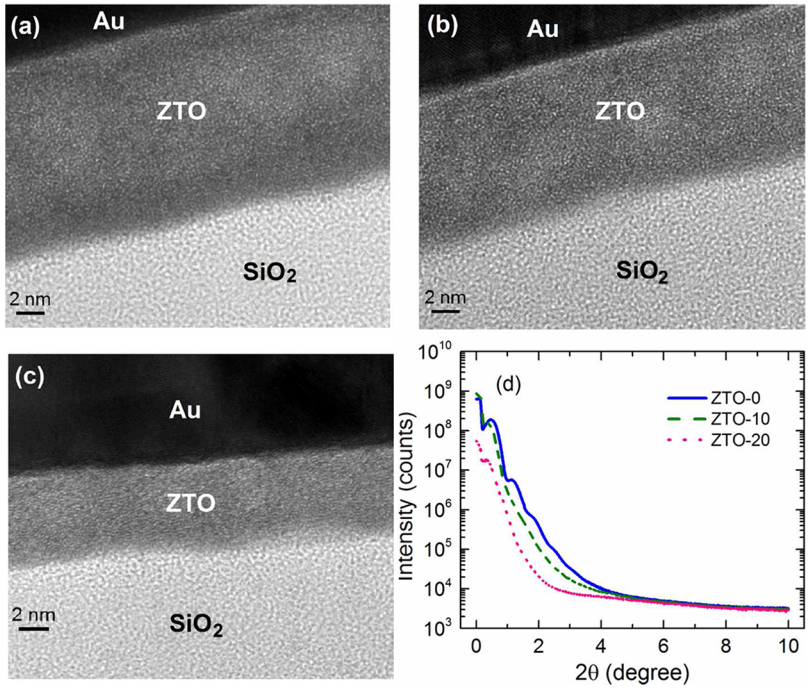

Figure 2. Cross-sectional TEM images of ZTO films soft-annealed for (a) 0 min (ZTO-0), (b) 10 min (ZTO-10), and (c) 20 min (ZTO-20). (d) X-ray reflectivity (XRR) patterns of the corresponding ZTO films.

arise because of the constructive and destructive interference of X-rays reflected from the two interfaces (here, air-ZTO and ZTO-SiO_2) as a consequence of the angular-dependent phase shift, were observed in the case of the ZTO-0 film. No fringes were observed in the case of the ZTO-10 and ZTO-20 films, which may be due to the smaller thickness of these films, as was observed from the TEM results. The thickness (t) of the films can be calculated from the period of Kiessig fringes using the following formula:

$$t = (i - j)\left(\frac{\lambda}{2}\right)\left(\frac{1}{\sin\theta_i - \sin\theta_j}\right)$$

where λ is the X-ray wavelength and θ_i and θ_j are the positions of the ith and jth interference maxima.[22] The thickness of the ZTO-0 film was calculated to be 12.8 nm, which is very close to the thickness value obtained from cross-sectional TEM image of the corresponding film. We would like to mention here that it was not possible to determine the thickness of ZTO-10 and ZTO-20 films from the XRR results, because of the absence of any interference fringes, but the TEM images clearly show the thickness values.

The O 1s XPS spectra of ZTO-0, ZTO-10, and ZTO-20 films on Si/SiO_2 surface are shown in Figure 3a. The obtained O 1s peaks were deconvoluted using Gaussian−Lorentzian (with 30% Lorentzian) profile, and the results are summarized in Table 1. The deconvolution of the O 1s peaks in all cases exhibited an intense peak at ∼530.3 eV, along with a broad shoulder peak at ∼531.8 eV. The peak at ∼530.3 eV is attributed to the oxygen in ZTO having no oxygen deficiency whereas the peak at ∼531.8 eV is attributed to oxygen-deficient regions in the ZTO system.[23,24] From the deconvoluted results summarized in Table 1, it is clearly seen that the area under the peak at ∼531.8 eV gradually increased with increasing soft annealing time and it was maximum in the case of the ZTO-20 film. The higher area under the peak at ∼531.8 eV indicates

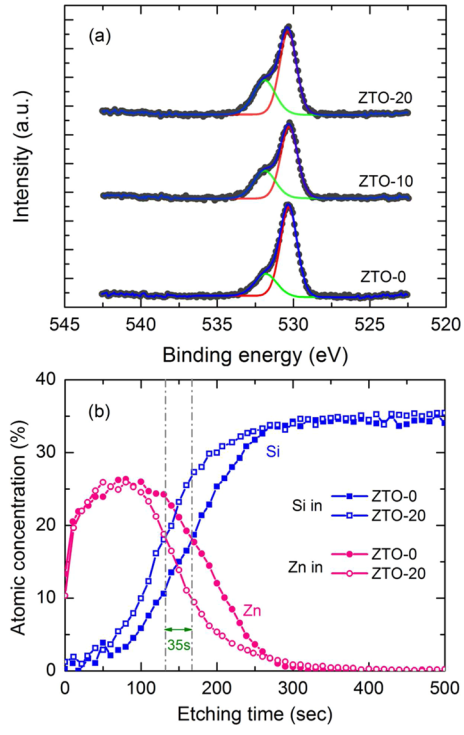

Figure 3. (a) O 1s spectra of different ZTO films and (b) depth profile of Si and Zn in ZTO-0 and ZTO-20 films.

that the ZTO-20 film contains a higher concentration of oxygen vacancies, compared to the ZTO-0 and ZTO-10 films. The depth profiles of Si and Zn in ZTO-0 and ZTO-20 films deposited on Si/SiO_2surface are shown in Figure 3b. It is clearly seen that a longer etching time (by ∼35 s) is required to see the same amount of Si in the case of the ZTO-0 film, compared to the ZTO-20 film. A similar difference in etching time was also observed by comparing the depth profile of Sn and Si (results

dx.doi.org/10.1021/am303235z | ACS Appl. Mater. Interfaces 2013, 5, 3587−3590

Table 1. XPS O 1s Peak Fitting Results of Different ZTO Films

peak position (eV)	full width at half maximum, fwhm (eV)	fractional area (%)
	Sample ZTO-0	
530.30	1.31	75.6
531.80	1.70	24.4
	Sample ZTO-10	
530.29	1.31	66.3
531.84	1.70	33.7
	Sample ZTO-20	
530.34	1.30	64.1
531.86	1.69	35.9

are not shown here). These results suggest that the thickness of ZTO-20 film is lower than that of ZTO-0 film, and this observation is consistent with the TEM and XRR results, as mentioned above. Similar behavior of (intermediate) thickness variation was also observed in the case of the ZTO-10 film, compared to the ZTO-0 film. From the TEM, XRR, and XPS results, it is confirmed that the thickness of the ZTO films decreased as the soft annealing time increased, which may be attributed to better atomic rearrangements such as the formation of Zn−O−Sn linkages, elimination of residual chemical species, and local densification before the high-temperature annealing. In contrast, without prolonged soft annealing, the Zn and Sn atoms undergo the oxidation process suddenly, as soon as the films were subjected to high temperature (500 °C) annealing, and not much time was allowed for the atomic rearrangement and densification, leading to a relatively higher film thickness.

Interestingly, the channel resistance of the ZTO TFTs was found to be lower as the soft annealing time increased. The value of channel resistance was found to be lowest in the case of the ZTO-20 TFT, in which the thickness of the channel layer was also lower, compared to the other two cases. The conductivity of oxide thin films has been reported to increase as the film thickness increased.[25,26] However, thinner films that were obtained as a result of higher soft annealing time in our present work showed lower channel resistance, compared to the thick films. From the O 1s XPS spectra, it is clearly seen that (i) the oxygen vacancy concentration in the case of soft-annealed ZTO films is higher than the ZTO films without soft annealing, and (ii) the ZTO-20 film contains the highest concentration of oxygen vacancies. It has been reported that the electrical conductivity in ZnO is mainly controlled by oxygen vacancies, which act as *n*-type donors.[27] Thus, the decrease in channel resistance in the case of thinner films, which was obtained as a result of soft annealing, can be attributed to the presence of a higher concentration of oxygen vacancies.

CONCLUSIONS

In summary, the impact of soft annealing time on the performance of solution processed amorphous ZTO TFTs was investigated. We find that the thickness of the ZTO channel layer decreases, while its conductivity increases, with increasing soft annealing time. The conductivity increase is shown to be a result of an increase in the oxygen vacancy concentration. We also find that an optimum soft annealing time exists for best device performance, which is ∼10 min for our devices.

AUTHOR INFORMATION

Corresponding Author

*E-mail: husam.alshareef@kaust.edu.sa.

Notes

The authors declare no competing financial interest.

ACKNOWLEDGMENTS

The authors acknowledge the generous support of the KAUST Baseline Fund.

REFERENCES

(1) Martins, R.; Fortunato, E.; Barquinha, P.; Pereira, L. *Transparent Oxide Electronics: From Materials to Devices*; Wiley: Chichester, U.K., 2012.

(2) Zhang, L.; Li, J.; Zhang, X. W.; Jiang, X. Y.; Zhang, Z. L. *Appl. Phys. Lett.* **2009**, *95*, 072112.

(3) Chiang, H. Q.; Wager, J. F.; Hoffman, R. L.; Jeong, J.; Keszler, D. A. *Appl. Phys. Lett.* **2005**, *86*, 013503.

(4) Yaglioglu, B.; Yeom, H. Y.; Beresford, R.; Paine, D. C. *Appl. Phys. Lett.* **2006**, *89*, 062103.

(5) Liu, J.; Buchholz, D. B.; Chang, R. P. H.; Facchetti, A.; Marks, T. J. *Adv. Mater.* **2010**, *22*, 2333.

(6) Chiu, C. J.; Chang, S. P.; Chang, S. J. *IEEE Electron Device Lett.* **2010**, *31*, 1245.

(7) Ong, B. S.; Li, C. S.; Li, Y. N.; Wu, Y. L.; Loutfy, R. *J. Am. Chem. Soc.* **2007**, *129*, 2750.

(8) Nayak, P. K.; Jang, J.; Lee, C.; Hong, Y. *Appl. Phys. Lett.* **2009**, *95*, 193503.

(9) Kim, H. S.; Byrne, P. D.; Facchetti, A.; Marks, T. J. *J. Am. Chem. Soc.* **2008**, *130*, 12580.

(10) Banger, K. K.; Yamashita, Y.; Mori, K.; Peterson, R. L.; Leedham, T.; Rickard, J.; Sirringhaus, H. *Nat. Mater.* **2011**, *10*, 45.

(11) Kim, M. G.; Kanatzidis, M. G.; Facchetti, A.; Marks, T. J. *Nat. Mater.* **2011**, *10*, 382.

(12) Nayak, P. K.; Pinto, J. V.; Goncalves, G.; Martins, R.; Fortunato, E. *J. Disp. Technol.* **2011**, *7*, 640.

(13) Avis, C.; Jang, J. *J. Mater. Chem.* **2011**, *21*, 10649.

(14) Kim, M. G.; Kim, H. S.; Ha, Y. G.; He, J. Q.; Kanatzidis, M. G.; Facchetti, A.; Marks, T. J. *J. Am. Chem. Soc.* **2010**, *132*, 10352.

(15) Lim, J. H.; Shim, J. H.; Choi, J. H.; Joo, J.; Park, K.; Jeon, H.; Moon, M. R.; Jung, D.; Kim, H.; Lee, H. J. *Appl. Phys. Lett.* **2009**, *95*, 012108.

(16) Nayak, P. K.; Busani, T.; Elamurugu, E.; Barquinha, P.; Martins, R.; Hong, Y.; Fortunato, E. *Appl. Phys. Lett.* **2010**, *97*, 183504.

(17) Nayak, P. K.; Hedhili, M. N.; Cha, D. K.; Alshareef, H. N. *Appl. Phys. Lett.* **2012**, *100*, 202106.

(18) Bong, H.; Lee, W. H.; Lee, D. Y.; Kim, B. J.; Cho, J. H.; Cho, K. *Appl. Phys. Lett.* **2010**, *96*, 192115.

(19) Wang, M. R.; Wang, J.; Chen, W.; Cui, Y.; Wang, L. D. *Mater. Chem. Phys.* **2006**, *97*, 219.

(20) Nomura, K.; Ohta, H.; Takagi, A.; Kamiya, T.; Hirano, M.; Hosono, H. *Nature* **2004**, *432*, 488.

(21) Nayak, P. K.; Jang, J.; Lee, C.; Hong, Y. *J. Soc. Inf. Display* **2010**, *18*, 552.

(22) Fewster, P. F. *Rep. Prog. Phys.* **1996**, *59*, 1339.

(23) Rim, Y. S.; Kim, D. L.; Jeong, W. H.; Kim, H. J. *Appl. Phys. Lett.* **2010**, *97*, 233502.

(24) Choi, J. Y.; Kim, S. S.; Lee, S. Y. *Appl. Phys. Lett.* **2012**, *100*, 022109.

(25) Jimenez-Gonzalez, A. E.; Urueta, J. A. S.; Suarez-Parra, R. *J. Cryst. Growth* **1998**, *192*, 430.

(26) Guo, E. J.; Guo, H. Z.; Lu, H. B.; Jin, K. J.; He, M.; Yang, G. Z. *Appl. Phys. Lett.* **2011**, *98*, 011905.

(27) Schoenes, J.; Kanazawa, K.; Kay, E. *J. Appl. Phys.* **1977**, *48*, 2537.